

Effects of poly(ethyleneimine) adsorption on graphene nanoplatelets to the properties of NR/EPDM rubber blend nanocomposites

Jeefferie Abd Razak^{1,2} · Sahrim Haji Ahmad¹ · Chantara Theyy Ratnam³ · Mazlin Aida Mahamood² · Noraiham Mohamad²

Received: 21 December 2014 / Accepted: 16 June 2015 / Published online: 26 June 2015
© Springer Science+Business Media New York 2015

Abstract The facile approach of non-covalent surface treatment utilizing poly(ethyleneimine) (PEI) polymer was applied to modify graphene nanoplatelets (GNPs). The effects of surface modification and various GNPs–PEI loadings to cure characteristic, mechanical, physical, and morphological properties of natural rubber (NR)/ethylene–propylene–diene–monomer (EPDM) blend nanocomposites were studied and compared to the unfilled NR/EPDM blend and blends filled with unmodified GNPs at similar loadings. We found that the modification of GNPs surface significantly influences the properties of NR/EPDM blends. The addition of GNPs significantly improved the blend's processability, offering approximately a 104.30 % increase in tensile strength obtained with the addition of 5.00 wt%

GNPs–PEI. A reduced swelling index of Q_f/Q_g in parallel with an increase in modified GNPs–PEI content revealed enhancements in terms of rubber–filler interactions between the NR/EPDM matrix and GNPs. These findings were further supported by X-ray diffraction, differential scanning calorimetry, thermogravimetry analysis, and fracture morphology by scanning electron microscope.

Introduction

Graphene, a basic unit of GNPs, is a monolayer of sp^2 -hybridized carbon atoms arranged in a two-dimensional lattice, which is considered a basic structural element of all graphitic carbons. Graphene has a large surface area and tunable surface properties, and exhibits a Young's modulus of 0.5–1 TPa [1], a breaking strength of 42 N m⁻¹ [2], an ultimate strength of 130 GPa, as well as thermal conductivity above 5000 W m K⁻¹ [3, 4]. Platelet thickness is in the range of 0.3–100 nm, while the density of GNPs is ~2 g cm⁻³. Hence, the higher aspect ratio combined with the extraordinary properties of GNPs qualifies them as an ideal reinforcing and functional filler for polymer nanocomposites (PNC) application [5–7]. The large surface area of GNPs increases the interface contact between the platelets and matrices, which could be beneficial for interfacial polarization [3]. In addition, the platelet's shape provides increased tortuosity for molecular transport which enhances the barrier properties of the resulted PNC [4]. However, an inert and hydrophobic graphene surface may not be compatible with many polymers. Dispersion of graphene nanosheets or platelets in polymer hosts and precise interface control are challenging due to their strong interlayer cohesive energy and surface inertia [8]. This renders graphene easy to agglomerate and re-stack into

✉ Jeefferie Abd Razak
jeefferie@utem.edu.my

Sahrim Haji Ahmad
sahrim@ukm.edu.my

Chantara Theyy Ratnam
chantara@nuclearmalaysia.gov.my

Mazlin Aida Mahamood
mazlin.aida@yahoo.com

Noraiham Mohamad
noraiham@utem.edu.my

¹ School of Applied Physics, Faculty of Science and Technology, Universiti Kebangsaan Malaysia, 43600 UKM Bangi, Selangor, Malaysia

² Carbon Research Technology Research Group, Engineering Materials Department, Faculty of Manufacturing Engineering, Universiti Teknikal Malaysia Melaka, Hang Tuah Jaya, 76100 Durian Tunggal, Melaka, Malaysia

³ Composites and Polymer Blends Group, Radiation Processing Technology Division, Malaysian Nuclear Agency, Bangi, 43000, Kajang, Malaysia

graphite through π - π stacking and van der Waals interactions since it is not able to repel the attractive forces between them due to the lack of intrinsic functional groups [9]. Thus, its surface must be first modified to provide it with suitable functional groups that are able to promote good dispersion and strong interactions with the chemical moieties in polymers.

Modifying the surface of graphene nanoplatelets can be achieved, either by covalent or non-covalent functionalization methods [10, 11]. Covalent treatment is severely prone to damaging the intrinsic properties of graphene, while non-covalent treatment normally preserves the pristine structure and properties of graphene. Non-covalent treatment normally preserves the intrinsic properties of graphene and will not reduce the intrinsic electrical and thermal conductivity of graphene. In this treatment method, surfactant, polyelectrolyte, and other organic molecules are used to enhance exfoliation and dispersion of graphene at various media through physical and electrostatic interactions. This could improve dispersion in non-polar polymers and other macromolecular structures by significantly reducing enthalpic interactions so that the dispersion in polymers is primarily driven by the system entropy [8]. In this study, surface modification to GNPs was achieved by utilizing a polymeric-based surfactant of poly(ethyleneimine) (PEI). PEI is a polycationic polymer containing a high density of ionizable tertiary, secondary, and primary amino groups in their molecular backbone. PEI is also highly water soluble due to ethylamine repeating units [12]. PEI can be electrostatically adsorbed on the negatively charged substrate to form the polyelectrolyte layer [13, 14]. The graphene sheets were able to assemble the active amino groups in PEI to further enhance the functionalization with some active groups, such as carboxyl or epoxy groups that further extends its application [13].

Fundamentally, an alternative simple route in developing new advanced engineering materials with improved properties is through the blending of two or more different rubbers. This method is more economically advantageous than synthesizing a new rubber compound, which is always associated with complex technical uncertainties. Rubber blending is prepared with specific objectives in mind, such as the enhancement of physical, chemical, and mechanical performance as well as the processing characteristics [12, 13]. However, there are many problems involving the compatibility and miscibility between the two rubber phases, which later tends to diminish the end performances of the blends. These include poor interfacial adhesion between rubber phases and uneven crosslinking distribution due to unbalanced saturation and polarity differences [12–15].

Hence, to improve compatibility and to stabilize the immiscible rubber blends, compatibilization using organic

molecules, block copolymers, or inorganic solid particles is often required [16]. Among all these alternatives, the addition of inorganic nanofiller to the blend is very promising due to its simplicity and the possibility of dual-functionality using added filler as a reinforcement agent or compatibilizer in the blend matrices. In order to optimize nanomaterial performance within matrices, surface modification or functionalization can be made prior to mixing of these constituents. This strategy will surely affect the interface interaction between the matrices and nanomaterial, and consequently contribute to better performance of the produced nanocomposites.

Over the past few years, many researchers have employed natural rubber (NR) and ethylene-propylene-diene-monomer (EPDM) synthetic rubber for the preparation of elastomeric blends [16–23]. Vulcanized NR/EPDM blend systems have been extensively studied because of their superior performance in tire application, as well as a significant improvement in heat and ozone resistance [22]. Despite having an attractive range of properties, excellent mechanical strength and elasticity, as well as good processing characteristic, the NR is highly unsaturated and is chemically reactive [13, 21, 24, 25]. Hence, NR rubber is highly susceptible to degradation and is very sensitive to environmental factors such as oxygen attack by ozone, light, moisture, humidity, radiation, and heat [17, 24, 25].

In the case of NR/EPDM rubber, poor environmental resistance behavior of the NR phase is significantly backed up by the presence of EPDM rubber phase, without sacrificing too much of NR's unique mechanical properties [26, 27]. Improvement in the poor ozone resistance of NR can be achieved by blending it with low-unsaturated rubbers such as EPDM (highly saturated and non-reactive) [19]. EPDM has an attractive balance of chemical, electrical, thermal, and mechanical properties [28]. EPDM offers good resistance to aging [29], weathering, oxidation, heat, oil, and chemical resistance, which are suitable characteristics for outdoor applications [18, 20, 28–32]. Blending of high-cost EPDM with low-cost NR offers economic advantages since an appreciable price difference is reached with outstanding results, which is normally the practice in various applications.

The presence of numerous functional fillers in NR/EPDM blends enhances the engineering properties and its functionalities [17, 19, 20, 22]. The addition of inorganic nanoparticles into an elastomeric blend is seen as interesting and straightforward since it can absorb strongly at the blend's interface and consequently is able to stabilize it [22]. The utilization of inorganic fillers for NR/EPDM has already been applied in previous studies. Previous examples of inorganic fillers are rice husk ash, silica [24, 32], carbon black [16, 20, 33–35], titania nanoparticles [22],

organo-modified Cloisite nanoclay [19], and more. However, to the best of our knowledge, there are still limited references available for NR/EPDM rubber blend or other polymeric rubber blend nanocomposites filled with graphene nanoplatelets [36–38]. Thus, this study provides an initiative in reporting the preliminary findings of preparation and characterization for NR/EPDM rubber blend filled with GNP nanocomposites that focuses on the effects of GNPs loading variations and non-covalent surface treatment of GNPs.

Materials and methods

Surface modification of GNPs

GNPs were purchased from Xiamen Graphene Technology Co. Ltd, China, with commercial trade name KNG-50. It has bulk density of $\sim 0.3 \text{ g cm}^{-3}$ with a true density of $\sim 2.25 \text{ g cm}^{-3}$ and specific surface area of $40\text{--}60 \text{ m}^2 \text{ g}^{-1}$. The overall carbon content for supplied GNPs was $> 99.5 \text{ wt}\%$, and it had a gray powder-like appearance. PEI was purchased from Sigma-Aldrich in the form of a viscous colorless liquid of branched polymer. The linear formula of PEI is $\text{H}(\text{NHCH}_2\text{CH}_2)_n\text{NH}_2$, and it has an average molecular weight (M_w) of $\sim 25000 \text{ g mol}^{-1}$, an average molecular number (M_n) of $\sim 10000 \text{ g mol}^{-1}$, and a density of 1.030 g ml^{-1} at $25 \text{ }^\circ\text{C}$. PEI was used without further purification. The chemical structure of PEI is depicted as shown in Fig. 1. For surface treatment medium preparation, the mixture of ethanol to distilled water was used at a ratio of 25:75 [39]. An overall volume of 1000 ml of solution mixture was prepared for every 2 g of GNPs and 3 g of PEI surfactant. High-speed stirring was performed at 1000 rpm, using a high-speed mechanical stirrer (model WiseStir HT50DX) with a combination of ultrasonication effects from the ultrasonic bath immersion setup (model JE10Tech UC-02). The process was performed for 5 h at a controlled temperature of $60 \text{ }^\circ\text{C}$. Later, the treated

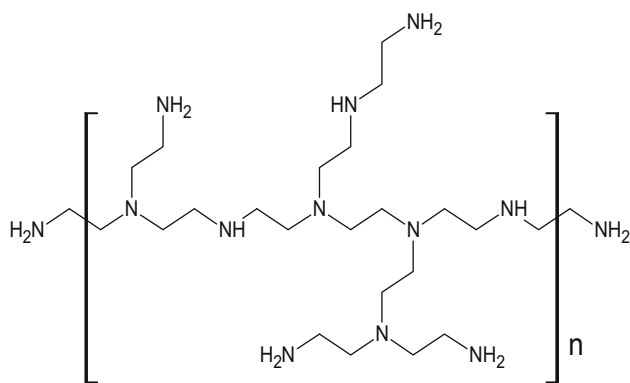


Fig. 1 The chemical structure of branched poly(ethyleneimine), PEI

GNPs were dried within 45 min at $100 \text{ }^\circ\text{C}$ and slowly stirred at 100 rpm using a hot-plate magnetic stirrer. Next, GNPs were filtered and washed using distilled water to remove the unreacted PEI, followed by oven heating at $150 \text{ }^\circ\text{C}$ and left for 5 h to allow for complete drying. The dried product was then ground using an agate mortar and placed in a close-sealed container. Modified GNPs were labeled as GNPs–PEI, while unmodified GNPs as uGNPs.

Characterization of uGNPs and GNPs–PEI

Spectroscopy analyses using Raman and FTIR were employed to evaluate the success of surface treatment on the GNPs. Raman spectra was obtained using a Horiba JobinYvon model HR800, utilizing a laser wavelength of 514.53 nm with a 10 mW power laser and a microscope objective of $100\times$ with an exposition of 3, accumulation of 5, and multi-spectro. The focal length used was 800 mm with a drift amount of $<0.015 \text{ nm s}^{-1}$. Fourier transform infra-red (FTIR) analysis was performed using JASCO FT/IR 6100 setup at 0.5 cm^{-1} resolution at the range of $4000\text{--}400 \text{ cm}^{-1}$ for 50 times scan laser type-II with a data interval of about 0.120529 cm^{-1} .

Morphological evaluation was performed using Field Emission Scanning Electron Microscopy (FESEM) and Transmission Electron Microscopy (TEM) to observe the transformations incurred due to the surface treatment. Morphological inspection of modified and unmodified GNPs was done using the TEM model Zeiss Libra 200 FE at 10 K magnification and FESEM model Hitachi SU8000 at 1 K magnification, and 2.0 kV accelerating voltage.

Melt compounding, cure characteristic, and preparation of NR/EPDM blends

Ethylene propylene diene rubber (EPDM) grade BUNA[®] EPT 9650 was procured from LANXESS, Pittsburgh, USA with Mooney viscosity UML (1 + 8) at $150 \text{ }^\circ\text{C}$ of $60 \pm 6 \text{ MU}$, ethylene content $53 \pm 4 \text{ wt}\%$, ENB content $6.5 \pm 1.1 \text{ wt}\%$ with volatile matter $\leq 0.75 \text{ wt}\%$, specific gravity 0.86, and total ash $\leq 0.50 \text{ wt}\%$ with a non-staining stabilizer. NR with commercial trade name of ‘SMR20’ was purchased from the Malaysian Rubber Board (LGM). The specification for SMR20 was 0.16 max. wt% dirt retained on 44 apertures, 1.00 max. wt% ash content, 0.60 max. wt% nitrogen, 0.80 max. wt% volatile matter, 30 min Wallace rapid plasticity (P_0), and 40 min. % of plasticity retention index (PFU). Both rubbers were masticated with a two-roll mill for about 10 min at $30 \text{ }^\circ\text{C}$ prior to their use. Other compounding ingredients, such as sulfur, zinc oxide, and stearic acid, were purchased from System/Classic Chemical Sdn. Bhd. Tetramethylthiuram disulfide (Perkacit-TMTD) was purchased from Aldrich Chemistry, while *n*-cyclohexylbenthiazolyl sulphenimide (CBS) and *n*-(1,3-

dimethylbutyl)-*n'*-phenyl-*p*-phenylenediamine (6PPD) were supplied by Flexys America, USA. Maleic anhydride (95% MAH) and bis(α,α -dimethylbenzyl peroxide) (98 % DCP) were supplied by Sigma-Aldrich, Germany. All compounding chemicals were used as received without further purification steps. The EPDM-*g*-MAH compatibilizer was synthesized using a melt-compounding method with peroxide-initiated grafting at 180 °C, 75 rpm of rotor speed for 5 min. This lab-scale preparation of EPDM-*g*-MAH compatibilizer was reported in our previous work [40, 41].

The melt-compounding process was performed in accordance to ASTM D-3192 for semi-EV sulfur vulcanization system [34, 42]. The formulation recipes used in the present study are shown in Table 1. The blends were compounded using a Haake PolyLab OS Rheodrive 16 internal mixer with a Banbury rotor at 0.70 fill factor and with overall 50 g of each blend formulation. The ratio of NR/EPDM, amount of EPDM-*g*-MAH compatibilizer, and internal mixer machine parameters had been optimized prior to this work and were reported elsewhere [39, 42, 43]. The melt-blending operation was performed at a mixing temperature of 70 °C and rotor speed of 70 rpm for 5 min. At first, NR, EPDM, and EPDM-*g*-MAH compatibilizer were blended for 1 min, before the first set of curatives was added, consisting of zinc oxide, stearic acid, and CBS. Later, unmodified or modified GNPs were compounded after 2 min into the mixing. GNPs were added to the blend compounds percentages of 0.00, 0.25, 0.50, 1.00, 3.00, and 5.00 wt% from the overall 50 g of NR/EPDM blend formulation recipe. Next, the second set of curatives consisting of an accelerator (6PPD and TMTD) and sulfur was mixed, 1 min before the end of the mixing period. The compound was dumped and left to cool at room temperature within 24 h before performing cure characteristic testing.

Table 1 Formulation recipe used in the preparation of NR/EPDM-filled GNPs blends

Materials	Compounds (phr) ^a
NR/EPDM	70:30
Zinc oxide	5.00
Stearic acid	2.00
6-PPD ^b	2.00
Sufur	1.50
CBS ^c	1.00
TMTD ^d	0.30

^a Parts per hundred

^b *N*-(1,3-Dimethylbutyl)-*N'*-phenyl-*p*-phenylenediamine

^c *N*-Cyclohexylbenthiazolyl sulphenimide

^d Tetramethylthiuram disulfide

The processability of NR/EPDM blends was then evaluated with cure characteristic assessment in accordance to ASTM D 2084 using an oscillating rotorless rheometer U-CAN Dynatex UR2010 (U-Can Incorporation, Taiwan). Samples of the respective blends were tested at 160 °C, 4.5 kg cm⁻² of compression pressure, 1.7 Hz of swing frequency, and +1° swing amplitude within 5 min of curing time. The maximum curing time (t_{c90}), scorch time (t_{s2}), minimum torque (M_L), and the maximum torque (M_H) were determined in this assessment. The cure rate index (CRI) and the torque difference ($M_H - M_L$) were calculated for further analysis of the blend's processability. The cure rate index (CRI) or the speed of the curing reaction was calculated using the following relation [32]:

$$\text{CRI} = \frac{100}{\text{Cure time} - \text{scorch time}} \quad (1)$$

The compounds of the rubber blend were subsequently molded with a compression machine at 160 °C and 150 kgf using a hot press (model GT7014-A, GoTech) based on the respective maximum cure time, t_{c90} obtained from the cure characteristic testing. The molded compounds were conditioned before testing and further analysis.

Tensile testing (ASTM D 1822) and shore-A hardness test (ISO 7691-1)

Tensile testing of NR/EPDM nanocomposite blends filled with uGNPs and GNPs-PEI was performed in accordance to ASTM D1822. A tensile test was conducted as a primary test in this study as it is relevant to the end applications [44]. The tests were performed using a Universal Testing Machine (model Toyoseiki Strogaph-R1) made in Japan. Dumb-bell shaped specimens of ~2.00 mm thickness were cut from the molded sheet using a SDL-100 (Japan) SD-type lever controlled sample cutter. The specimens were tested at a crosshead speed of 500 mm min⁻¹, and the tests were performed at 23 ± 2 °C. At least seven samples from each formulation were tested to ensure a high confidence level in the experimental results. Tensile properties such as tensile strength (TS); modulus at 100, 300, and 500 % of elongation (M100, M300, and M500); and the percentage of elongation were determined in this study (%E). The following equation was used for the calculation of %E value [32]:

$$\text{EB} = \frac{\text{Displacement at failure}}{\text{Effective gauge length}} \times 100. \quad (2)$$

The hardness measurements of the NR/EPDM nanocomposite blend samples were done according to ISO 7691-1 using a manual durometer hardness tester (Zwick-Roell 3114) type Shore-A. About five reading points were taken from every sample for averaging purposes.

Swelling, crosslink density, and rubber–filler interaction of NR/EPDM blends

Swelling tests of cured NR/EPDM blend nanocomposite samples were performed in accordance with ISO 1817. Samples with dimensions of 20 mm length × 20 mm width × 2 mm thickness were weighed using an electronic top loading balance (model AB135-S/FACT, Mettler Toledo). Later, samples were immersed in toluene in a dark environment 72 h at 25 °C until the equilibrium was achieved [23]. The swollen samples were taken out after the immersion period and were weighed again. The change in mass is referred to as the percentage of swelling and is given in the following Eq. 3 [45]:

$$\text{Swelling}(\%) = \frac{(W_2 - W_1)}{W_1} \times 100, \tag{3}$$

where W_1 is the initial mass (g) and W_2 is the mass (g) after toluene immersion. By applying the Flory–Rehner equation (Eqs. 4–6), the molecular weight between crosslinks (M_c) and the crosslink density (V_c) or the concentration of elastically of effective chains can be calculated based on the swelling test results. These parameters include the true chemical crosslinks and physical crosslinks such as chain entanglements and loops [23].

$$M_c = \frac{-\rho_p V_s V_r^{1/3}}{\ln(1 - V_r) + V_r + \chi V_r^2}, \tag{4}$$

$$V_r = \frac{1}{1 + Q_m}, \tag{5}$$

$$V_c = \frac{1}{2M_c}, \tag{6}$$

where ρ is the rubber density ($\rho_{NR} = 0.92 \text{ g cm}^{-3}$; $\rho_{EPDM} = 1.06 \text{ g cm}^{-3}$), V_s is the molar volume of the toluene ($V_s = 106.4 \text{ cm}^3 \text{ mol}^{-1}$), V_r is the volume fraction of the polymer in the swollen specimen, and Q_m is the weight increase of the blends in toluene and χ is the interaction parameter of the rubber network–solvent (χ of NR = 0.393; χ of EPDM = 0.49). For rubber–filler interactions or the swelling index, the Lorenz and Park equation was applied [46].

$$\frac{Q_f}{Q_g} = ae^{-z} + b, \tag{7}$$

where subscripts f and g refer to filled and gum vulcanizates, respectively, and z is the ratio by weight of the filler to the rubber matrix in the vulcanizates, and a and b are the constants. The higher the Q_f/Q_g values, the lower the extent of the interaction between the filler and the matrix.

In this study, the weight of toluene uptake per gram of rubber matrix (Q) is as follows [47]:

$$Q = [(W_s - W_d)/W_i] \times 100/92.15 (\%), \tag{8}$$

where W_s is the swollen weight, W_d is the dried weight, and W_i is the original weight.

GNPs dispersion analysis using X-ray diffraction (XRD) method

X-ray diffraction (XRD) was carried out using PanAnalytical diffractometer operating with Cu K α radiation ($\lambda = 0.154 \text{ nm}$) at 40 kV and 30 mA. Scans were taken from 20° to 60° with a continuous scan step size of 0.0170°. Samples for modified and unmodified GNPs were prepared in powder form, whereas the NR/EPDM rubber blend nanocomposites were prepared from the residue of vulcanized compression molded rubber, at least ~1.00 mm thick. Full-width-at-half-maximum (FWHM) and d -spacing parameters were highlighted to evaluate the effects of GNPs surface modification and the amount of GNP loadings of produced nanocomposites.

Heat flow analysis using differential scanning calorimeter (DSC)

Heat flow analysis was carried out using a DSC machine (model Jade by Perkin Elmer). Analysis was performed in the temperature range of –65 to 150 °C under a heating rate of 20 °C min⁻¹ with nitrogen gas continuously purging at a flow rate of 20 ml min⁻¹. About ~10.00 mg of sample was weighed and put in a crimped standard aluminum pan. The first heating endotherms were analyzed to understand the influence of GNPs modification and amount of loading to the heat flow behavior of the produced blends. The glass transition temperature (T_g) was determined from the primary point that intersected the tangent discontinuity in the DSC curve [43].

Thermal degradation and residue evaluation using thermogravimetric analysis (TGA)

The thermal behavior of produced blends was further analyzed using TGA. This analysis was performed to observe the degradation behavior and residue evaluation for NR/EPDM blends in relation to filler surface modification and the amount of loadings. The blend was cut into small pieces and was weighed to be around ~10 mg, and placed into a crucible. Samples were tested using TGA–DTG Rigaku TG8120 Thermo Plus Evo machine and operated between 30 and 600 °C temperature range at a heating rate of 10 °C min⁻¹ under atmospheric nitrogen conditions.

Tensile fracture morphology observation using scanning electron microscope (SEM)

The selected tensile-fractured sample from each NR/EPDM blend formulation was adhered on the aluminum stub with carbon tape. Later, the samples were sputter coated with a thin layer of gold using Polaron E-1500 sputter coater equipment. The morphologies of NR/EPDM

blends filled with modified and unmodified GNPs and the unfilled blends were observed at 1 K magnification using the variable pressure scanning electron microscope (VPSEM model Zeiss Evo) operated at 15 kV accelerating voltage with a secondary electron (SE) mode signal detector.

Results and discussion

Characterization of uGNPs and GNPs–PEI

Spectroscopy characterization for the uGNPs and GNPs–PEI was performed using Raman and FTIR method to evaluate the success of the surface treatment done to GNPs. Raman and FTIR spectroscopy for uGNPs and GNPs–PEI are presented in Figs. 2 and 3, respectively.

In Raman spectra for the uGNPs and GNPs–PEI samples, three characteristic peaks appeared at ~ 1370 – 1375 cm^{-1} (D band), ~ 1600 – 1610 cm^{-1} (G band), and ~ 2710 – 2740 cm^{-1} (2D band). We found that the intensity of the G band and D band for the GNPs–PEI sample became weaker than with uGNPs, indicating a higher level of disorder and formation of defects in the modified graphene layers due to the treatment. A higher G band value for uGNPs implies the intact nature of GNPs' graphitic domain, while the D band is a characteristic of defects and disorder. However, it was found that the intensity ratio from I_d to I_g of non-covalent-treated GNPs–PEI was markedly decreased (I_d/I_g 0.250) compared to uGNPs (I_d/I_g of 0.314). The lower I_d/I_g ratio of GNPs–PEI was corresponded to a high structural integrity of modified GNPs, as mentioned in previous work [11]. Hence, the non-covalent treatment performed to GNPs not only introduced interruptions in platelet's stacks and defects, but also improved the structure of modified GNPs due to PEI adsorption.

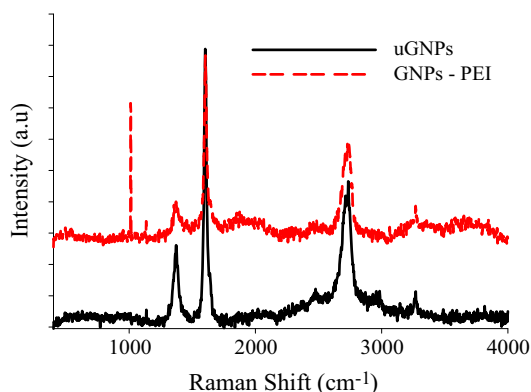


Fig. 2 Raman spectra of uGNPs and GNPs–PEI

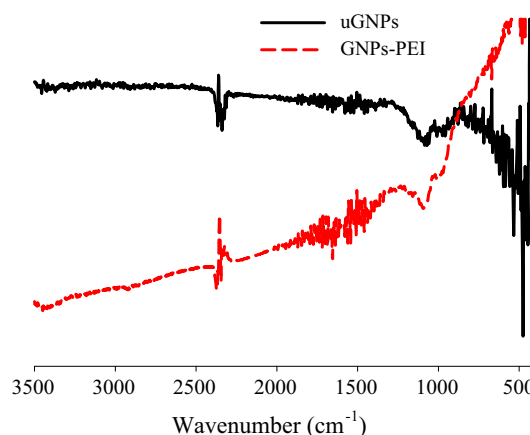


Fig. 3 FTIR spectra of uGNPs and GNPs–PEI

In addition, the region of 1050 – 1200 cm^{-1} is due to the vibration of the C–NH₂ group [48]. An identical peak obtained at 1013.82 cm^{-1} in the GNPs–PEI sample referred to the twisting of the CH₂ groups while the 1135.48 cm^{-1} peak indicated the C–C stretching mode that is known to mix with the methyl rocking mode, giving rise to the Raman band which overlapped with the asymmetric NH₂ bending vibrations by adsorbed PEI [48]. These may explain the occurrence of adsorption between GNPs and PEI polymers through non-covalent interaction. An additional polymeric carbon chain adsorbed on the GNPs surface may enhance the surface chemistry of modified GNPs samples. The presence of surface defects and adsorbed polymer in GNPs–PEI may provide an additional benefit to the mechanical interlocking improving rubber–nanofiller interactions between the GNPs surface and rubber blend matrix when they are incorporated together.

For FTIR spectral analysis, we found two available distinct peaks that corresponded to the skeletal C–C stretching of ethyl group or C–O stretching at ~ 1069 cm^{-1} and the presence of hydroxyl group (–OH stretching) at ~ 2365 cm^{-1} , for both uGNPs and GNPs–PEI [49]. These hinted that the mass production of GNPs was originally made from the acid treatment. FTIR spectra for GNPs–PEI experienced the presence of a new weak band at 966.16 cm^{-1} which referred to the skeletal motion of the C–C backbone, indicating an adsorption of the polymeric PEI into GNPs surface that is likely to disturb the arrangement of atomic carbons in the hexagonal lattice of graphene platelets due to small changes in the dipole moment associated with their vibration [49]. In addition, the presence of a new peak at 2322.00 cm^{-1} for GNPs–PEI confirmed the interaction between PEI and GNPs surface through the formation of hydrogen bonding that was present in the multiple structures of –OH associated with the carboxylic acids. The presence of these two new peaks

further supports the success of GNPs non-covalent treatment.

Morphological observation by FESEM and TEM was performed to identify the transformation that occurred due to surface modification of GNPs. The FESEM images of uGNPs and GNPs–PEI are presented in Fig. 4a, b. We found that a longer ultrasonication exposure and high-speed mechanical shearing action had caused an enhancement between the GNPs–PEI platelet layer spacings as compared to uGNPs. A sudden decrease in lateral dimension and thickness of GNPs–PEI layers was obviously detected, whereby the average largest in-plane lateral dimension was approximately about $\sim 1220.67 \pm 197.63$ and $\sim 301.47 \pm 38.84 \mu\text{m}$ for uGNPs and GNPs–PEI, respectively. Reductions in GNPs dimensions decreased the interlayer cohesive energy that could possibly promote good dispersion of filler within the polymer matrix [8]. Further, in terms of the exfoliation between the layers, GNPs–PEI possessed better platelet separation compared to unmodified GNPs.

TEM observations at 10 K magnification for both uGNPs and GNPs–PEI samples are depicted in Fig. 5a, b. GNPs exhibited a layered structure with stacked graphene sheet morphology. It was found that uGNPs layers were obviously darker than GNPs–PEI, representing a closely spaced platelet stack due to agglomeration and the graphitic nature of GNPs. However, some spots in the captured image of uGNPs (Fig. 5a) show a transparent and thin layer of graphene platelet surface with the presence of crumple folding edges and wrinkled graphene morphology. These indicate the flexible nature of platelets that is beneficial as an elasticity improver in any filled composite application. Enhanced platelet translucency in modified GNPs–PEI as shown in Fig. 5b may indicate the occurrence of polymeric PEI adsorption to the surface of GNPs by wrapping mechanism. The well-distributed nano-sized darker dots on GNPs surface were the PEI polymers that were already trapped and non-covalently bonded within GNPs lattices and basal surfaces. The segregated PEI between the platelet interlayers may further contribute in the stacking separation and platelet intercalation, and also

in lowering the surface tension of GNPs that could prevent agglomeration due to steric repulsive forces of GNPs [50].

The morphological behavior of GNPs before and after the surface modification was further evaluated through an XRD analysis. As depicted in Fig. 6, both uGNPs and GNPs–PEI showed an intense diffraction peak at 26° – 27° that corresponded to basal spacing of graphite with d -spacing of ~ 0.335 nm. However, a slight intensity decrease and shift in an identical peak of GNPs–PEI indicated that the treatment reduced the graphite crystallinity. This showed that the adsorption or wrapping of PEI into GNPs may occur at the outermost sheets of the stacked aggregates, or partially intercalated where several graphene planes remain in pristine form. Conversely, uGNPs experienced a lower full-width-at-half-maximum (FWHM) at higher d -spacing values than GNPs–PEI. Increased FWHM values with certain peak broadening for GNPs–PEI at 0.8029 represent a successful platelet separation between GNPs layers, while the decrease d -spacing value at 0.3380 nm may indicate an occurrence of polymeric adsorption between each layer that introduced another thickness layer by polymeric coating which non-covalently bonded to the GNPs surface.

Processability evaluation of NR/EPDM blends by cure characteristic studies

Cure characteristics testing was conducted to determine how well the blended compounds mixed and how the blend will process and cure in the next processing stage [44]. The curemeter measures the increasing resistance to distortion and flow as crosslinks develop in the material [44]. Cure characteristics studies provide information on scorch time (t_{s2}), maximum molding time (t_{c90}), minimum torque (M_L), maximum torque (M_H), torque difference ($M_H - M_L$), and cure rate index (CRI). The processability of NR/EPDM blend nanocomposites is reported and summarized in Table 2.

t_{s2} is the time required for the cure state to increase to two torque units above the minimum at a given cure temperature, and often correlates well with the Mooney scorch

Fig. 4 FESEM images of **a** uGNPs and **b** GNPs–PEI

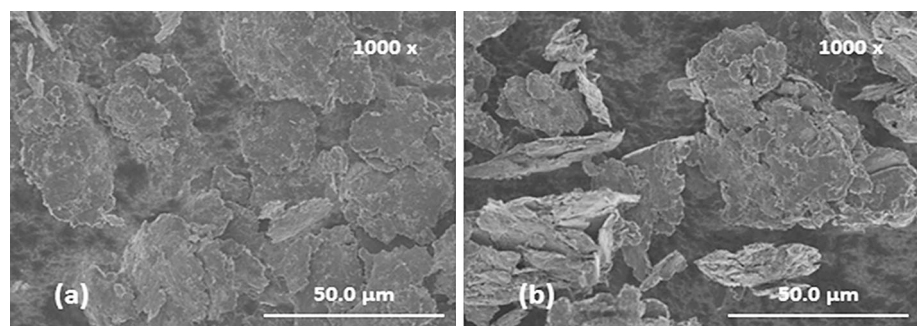


Fig. 5 TEM images of **a** uGNPs and **b** GNPs–PEI

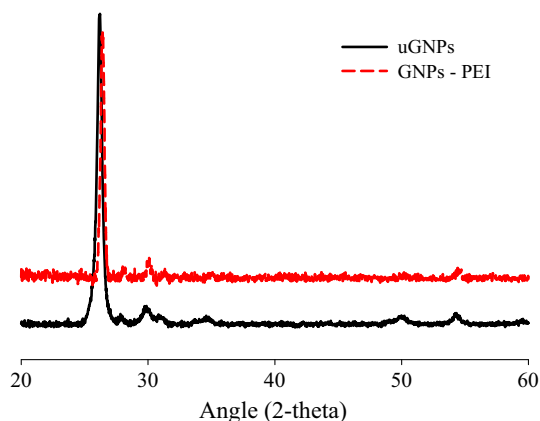
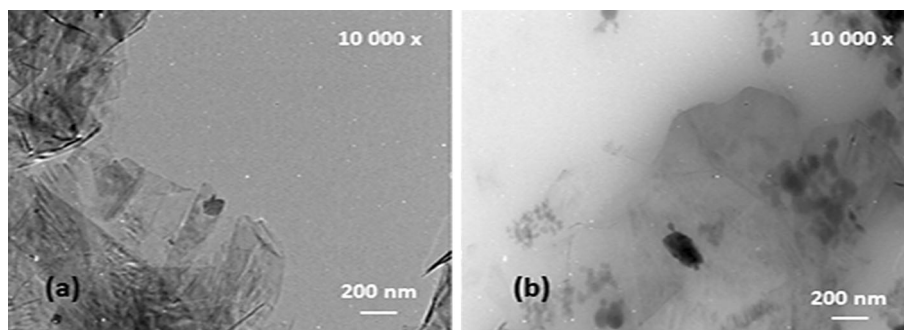


Fig. 6 XRD diffractograms of uGNPs and GNPs–PEI

time [23]. For t_{s2} , the scorch safety of NR/EPDM blends filled with GNPs–PEI experienced a stable decreasing pattern with an increase in GNPs loadings. Nanocomposites with GNPs–PEI addition possessed a shorter scorch time than uGNPs-filled NR/EPDM blends. It is understood that during the scorch delay period, the majority of the accelerator chemistry took place [51]. At this point, it is

believed that the addition of GNPs–PEI could promote fast curing phenomena of NR/EPDM blends due to high thermal conductivity induced by GNPs nanomaterial. Further, the polymeric layer of PEI adsorbed on the GNPs surface acted as an active point for better rubber–filler interactions. Hence, the lower scorch time following the addition of GNPs–PEI was due to active surface chemistry of GNPs–PEI as compared to uGNPs-filled blend system which gives a high surface area and high graphene nanoplatelets structure.

t_{c90} is the time required to reach 90 % of full cure, and this is generally the state of cure at which most physical properties reach their optimum. It was found that the t_{c90} decreased with the increased of GNPs loading for both NR/EPDM blends, either filled with uGNPs or GNPs–PEI. However, blends incorporated with GNPs–PEI possessed lower t_{c90} values at all loading amounts compared to blends filled with uGNPs. This indicated that modifications to GNPs eliminated the hindrance to interactions between the rubber blend and nanofiller, due to improved solubility of GNPs–PEI. Modified GNPs–PEI experienced a reduction in their lateral dimension size together with additional surface chemistry on GNPs by PEI. Both scenarios may

Table 2 Cure characteristics studies for NR/EPDM rubber blends filled with various wt% loadings of uGNPs and GNPs–PEI

Output	System	0.00 wt%	0.25 wt%	0.50 wt%	1.00 wt%	3.00 wt%	5.00 wt%
t_{s2} (min)	A ^a	2.460	2.370	2.395	2.355	2.330	2.175
	B ^b	2.460	2.250	2.067	1.733	1.109	0.883
t_{c90} (min)	A	3.200	3.060	3.100	3.035	2.985	2.825
	B	3.200	2.933	2.750	2.375	1.559	1.325
CRI (min^{-1})	A	135.135	144.928	141.844	147.059	152.672	153.846
	B	135.135	146.431	146.413	155.763	222.222	226.244
M_L (dNm)	A	6.590	6.495	6.575	6.665	6.545	6.965
	B	6.590	6.200	6.790	7.085	8.160	8.485
M_H (dNm)	A	20.055	20.245	20.035	19.845	20.700	20.880
	B	20.055	20.325	20.785	20.975	21.265	21.315
$M_H - M_L$ (dNm)	A	13.465	13.750	13.460	13.180	14.155	13.915
	B	13.465	14.125	13.995	13.890	13.105	12.830

^a NR/EPDM blends filled with uGNPs

^b NR/EPDM blends filled with GNPs–PEI

assist crosslink formation during the vulcanization time by promoting the accelerator systems to interact to each other for polysulfide formation [52]. Hence, adding GNPs–PEI tends to reduce t_{c90} and t_{s2} or accelerate the vulcanization process, but still efficiently cures the NR/EPDM blends [24, 27].

The cure rate index (CRI) is a measurement of the vulcanization rate based on the differences between the t_{c90} and t_{s2} . There was no considerable variation noted in the CRI for NR/EPDM blends filled with uGNPs. The CRI decreased slightly when about 0.50 wt% of uGNPs were added to the NR/EPDM blend. This may be due to cure incompatibility effects caused by the decrease in reactive sites on the rubber molecules available for crosslinking reactions [23]. On the other hand, the CRI for NR/EPDM blends increased with GNPs–PEI loadings, which may indicate reduced activation energy for crosslink formation [53] and increased interaction sites for vulcanization [32].

M_L is the minimum torque in the rheometer that often correlates well with the Mooney viscosity of a compound [52], while M_H is the maximum torque that was achieved during the curing time [51]. M_L is commonly considered as a representative of the uncured stock's elastic modulus and also provides valuable information about a compound's processability [23], while M_H indicates the vulcanized strength of rubber blend compounds or the degree of crosslinking in the elastomer [52]. The higher the torque obtained, the higher the number of crosslinks created [54]. Addition of GNPs–PEI increased the M_H and M_L at a linear pattern of increased filler loading. For M_L , the fluctuating pattern of processing load at both lower and higher uGNP loading may indicate less processability for NR/EPDM blends filled with uGNPs. Higher M_L and M_H values for NR/EPDM blends filled with GNPs–PEI compared to NR/EPDM blends filled with uGNPs indicate adequate filler wetting characteristics due to improved GNPs–PEI interaction with NR/EPDM macromolecules network. Polymer chain segment spreading has been shown to increase as the filler content increases for blends filled with GNPs–PEI. The incorporation of GNPs–PEI increases the processing load due to increased flow resistance, caused by smaller sized GNP platelets and the formation of “house-of-cards” structures, in which edge-to-edge and edge-to-face interactions between the dispersed layers form percolation structures. In effect, this factor increasingly restricts the molecular mobility of macromolecules thus resulting in an increase in the processing torque behavior [52].

The difference between $M_H - M_L$ is a measure of the shear dynamic modulus that indirectly relates to the state of cure or crosslink density of the NR/EPDM rubber blends [17, 21]. It is also the extent of vulcanization and attainment of a characteristic network chains [52]. It is well understood that the blending of highly unsaturated NR and highly saturated

EPDM generally leads to a cure mismatch, resulting in an uneven crosslink density distribution and with it, inferior mechanical properties [23]. This could be a predominant reason for the fluctuating pattern of torque differences for NR/EPDM blends filled with uGNPs filler. Conversely, blends filled with GNPs–PEI experienced a stable and linear decreasing pattern of torque difference. The drop-off pattern indicates a decrease in the resultant blend crosslink density with an increase of GNPs–PEI filler addition. The presence of an additional polymeric PEI layer that adsorbed and wrapped on the GNP surface provides a barrier between the blend and filler which reduces the crosslink formation among the rubber phases, but may increase the chemical interactions between them through other specific phenomena of enhanced compatibilization due to the addition of an inorganic filler. This situation could be confirmed through a systematic swelling testing, the analysis of which shows an agreement with the findings obtained from the cure characteristic studies of torque difference.

Mechanical properties of NR/EPDM blends nanocomposites

In this study, the mechanical properties of NR/EPDM blends were assessed through tensile properties characterization and Shore-A hardness test as a function of GNP loading and surface treatment. NR/EPDM-filled unmodified uGNPs blends (system A) and NR/EPDM-filled modified GNPs–PEI blends (system B) were tested. The experimental data are tabulated in Table 3. The results clearly show that the tensile strength (TS), elongation at break (EB), and modulus at 100, 300, and 500 % elongation (M100, M300, and M500) increase with an increase in both uGNPs and GNPs–PEI. Blends filled with GNPs–PEI experience a slightly higher result and improvement across all tensile properties compared to unfilled NR/EPDM blends and NR/EPDM blends filled with uGNPs at all loadings.

For instance, the TS drastically increased to 104.3 % improvement as compared to the unfilled blend, when 5.00 wt% of GNPs–PEI was added. However, a reduction in TS was encountered for blends filled with higher uGNP content due to agglomeration and aggregation of platelets that enables pre-mature failure, as observed in Fig. 10b of SEM fracture morphology observation. NR/EPDM blends filled with uGNPs maximally survived up to 3.00 wt% of uGNPs, offering maximum performance of TS where it produced an 87.6 % improvement compared to unfilled NR/EPDM blend.

Surface modification of GNPs using PEI succeeded in improving the mechanical performance of NR/EPDM blends. The polymeric layer of PEI was adsorbed to the GNPs surface and may have created retention effects among GNPs, enhancing the separation between them.

Table 3 Tensile properties and shore-A hardness values for NR/EPDM rubber blends filled with uGNPs and GNPs–PEI at various filler loadings

Output	System	0.00 wt%	0.25 wt%	0.50 wt%	1.00 wt%	3.00 wt%	5.00 wt%
TS (MPa)	A ^a	7.322	7.970	9.119	11.378	13.738	10.702
	B ^b	7.322	8.890	10.356	11.277	13.843	14.959
EB (%)	A	774.687	784.022	896.987	1007.268	1079.738	902.778
	B	774.687	858.187	950.642	1018.913	1057.725	1110.337
M100 (MPa)	A	1.080	1.108	1.155	1.172	1.481	1.607
	B	1.080	1.428	1.437	1.480	1.610	1.529
M300 (MPa)	A	2.046	2.060	2.273	2.313	2.967	3.233
	B	2.046	2.913	3.036	3.127	3.165	3.249
M500 (MPa)	A	4.375	4.621	4.978	5.289	6.343	7.663
	B	4.375	8.032	8.596	8.968	11.108	9.534
Shore-A	A	45.550	46.100	47.450	48.000	48.700	49.550
	B	45.550	46.500	47.550	47.650	47.750	49.850

^a NR/EPDM blends filled with uGNPs

^b NR/EPDM blends filled with GNPs–PEI

Polar interactions between GNPs–PEI sheets and polar polymer matrices were introduced by oxygen-containing groups in the platelets. This directly caused an improvement in filler dispersion within the NR/EPDM blends [55]. On the contrary, limited functional groups that were available in uGNPs surfaces caused a selective distribution of GNPs into high-polarity phases of NR instead of EPDM phase. This created an uneven tensile loading and later caused a reduction in TS and EB for NR/EPDM blends at 5.00 wt% uGNPs addition. Furthermore, no or limited functional groups at uGNPs surfaces made them hydrophobic, and the nature of the highly specific surface area of uGNPs facilitated an irreversible aggregation or even restacking to graphite through strong π – π stacking and van der Waals interactions, greatly limiting the application of uGNPs in numerous areas [56].

For EB, an overall improvement pattern was obviously similar to TS. System A experienced a major decrease in EB value due to the saturation effect and agglomeration of GNPs that may have induced weak points, which could facilitate a pre-mature failure during applied stress. At higher uGNPs loadings, the added filler failed to support the stress transferred from the matrix, suggesting poor interfacial interactions between uGNPs and NR/EPDM matrices. Poor adherence in the filler matrix could give rise to the formation of voids in the interphase, which would decrease the mechanical properties of filled rubber [27]. Moreover, the separation and dispersion of uGNPs at higher loading may not be assisted by high viscosity and molecular weight of NR/EPDM blends, which reduces the ductility of produced samples.

NR/EPDM blends from system B had an EB value that was appreciably higher than system A's blends. The addition of GNPs to NR/EPDM blends may affect crosslink formation by enhancing the macromolecular distance and space between the crosslinks, causing free mobility between the

chains of the stretched samples. This situation may further assist the slippage of GNPs and rubber blend macromolecules that consequently further enhance the elasticity and macromolecular chain crystallization of blend samples. An extraordinary increase in EB with the increase of GNPs filler loading is ascribed to the fact that some rubber chains are not fully cross linked with sulfur in the presence of platelets layers, and these uncrossed chains are responsible for the incremental elongation of nanocomposite samples which develop into breaks [19]. Alternatively, it is known that GNPs have a 2-D multilayer structure, in which a unique frictional sliding interlayer normally exists due to the fact that graphene layers within GNPs are only bonded with weak van der Waals forces [3]. Thus, higher loading of GNPs provides a greater possibility of EB being assisted due to the interlayer sliding of nanoplatelets.

The stiffness behavior of NR/EPDM blends filled with GNPs was investigated through the evaluation of modulus at 100, 300, and 500 % of elongation. Increases in M100, M300, and M500 of NR/EPDM blends filled with either GNPs–PEI or uGNPs nanofiller are the manifestation of the reinforcing ability of GNPs in the NR/EPDM rubber matrix. This finding was consistent with previous work by many researchers on other rubber blend systems filled with various types of filler [18, 24, 25]. It is interesting to note that the improvements in M100, M300, and M500 for NR/EPDM blends filled with GNPs–PEI were larger than NR/EPDM blends filled with uGNPs at all loadings. This may be attributed to the lamellar structure of graphene that allows for better wettability and enhances rubber–nanofiller interactions due to hydrogen and van der Waals forces of non-covalent-modified GNPs, thereby leading to a better stress transfer for improved nanocomposites stiffness [7, 44].

Shore-A hardness of both systems A and B showed an increasing pattern of hardness value with increasing GNPs

loadings. Hardness for unfilled NR/EPDM blends was lower than with filled blends. However, there was no obvious significant difference between the hardness of both system A and B at each GNPs loading as the difference in values was insignificant. Shore-A hardness represents the resistance of materials toward the local indentation due to a given applied force. For this study, the measurement of hardness can be related with the crosslink behavior of produced nanocomposites. Hence, it can be clearly justified that an addition of either modified or unmodified GNPs will change the crosslinking characteristics of the blends due to loadings variation, whereas the treatment done to the nanofiller do not give any clear impact on this physical attribute.

Swelling, crosslink density, and rubber–filler interaction of NR/EPDM blends

The percentages of swelling {A} and the crosslink density {B} for NR/EPDM blends filled with uGNPs and GNPs–PEI are shown in Fig. 7. It was found that the plots for both attributes were mutually intersected and opposite of each other. The crosslink densities were enhanced with the decrease of swelling percentage. This situation was applied for both systems A and B of the produced blends. However, it was interesting to note that the blends filled with GNPs–PEI had less swelling percentage but higher crosslink density compared to blends filled with uGNPs. For example, NR/EPDM blend filled with 5.00 wt% of GNPs–PEI had about 3.84 % lower swelling percentage and 17.31 % higher crosslink density compared to NR/EPDM blend filled with uGNPs at a similar loading. The higher the crosslink density of the rubber composite, the lower the percentage of swelling for vulcanized rubber in a given solvent [52].

Lower swelling percentages in the presence of modified GNPs–PEI filler can be explained by the possibility of increased crosslink density and improved rubber–filler interactions. This phenomenon has further obstructed the

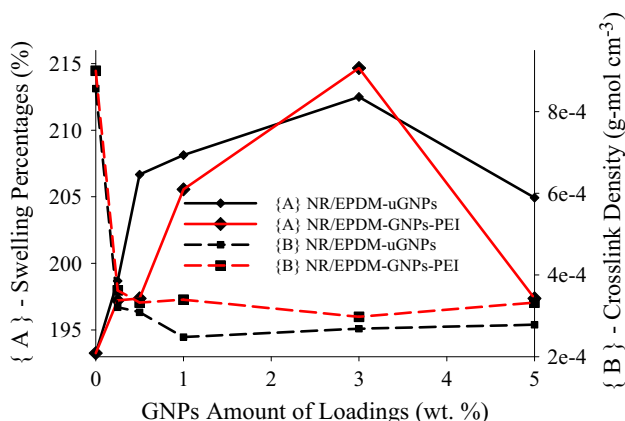


Fig. 7 Correlation plot between the swelling percentages and crosslink densities of NR/EPDM blends filled with uGNPs and GNPs–PEI

penetration of solvents. Further, an improved GNPs–PEI dispersion may have created a tortuosity path that reduces the transport area within the blends [57]. Swelling takes place when the osmotic pressure exerted on the rubber blend by the solvent is stronger than the cohesive forces between the rubber molecules. Hence, the osmotic pressure exerted on the rubber by the solvents falls as the molecular weight of the rubber increases with crosslinking [52].

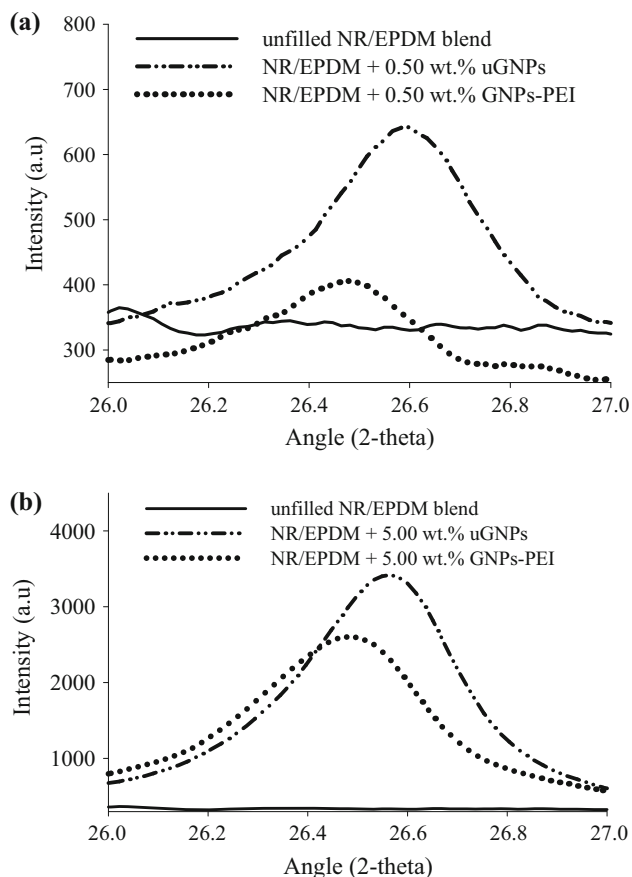
Subsequently, the interactions between rubber–filler GNPs and NR/EPDM blends were determined through the measurement of toluene uptake per 100 g of rubber and swelling index calculation based on Lorenz and Park equation [46]. The results are summarized in Table 4. A higher swelling index reflects lower molecular interactions between the filler and the rubber blend matrices. It was found that NR/EPDM blends filled with GNPs–PEI, as in system B, possessed a lower Q_p/Q_g value than system A at all loadings. This situation could be related to the extensive distribution of GNPs at the molecular level in the rubber matrix [52]. The molecular contact between GNPs–PEI and NR/EPDM matrices became greater with an increase in GNP loading, due to an active surface chemistry of modified GNPs, as observed during cure characteristic studies on scorch time reduction due to GNPs–PEI addition (Table 2). It is suggested that certain rubber–filler bonding or state of adhesion between two rubbers and GNPs were established and hence caused fewer opportunities for the solvent to pass through the rubber macromolecules, significantly dropping the swelling behavior and increasing the resistance of produced blends toward chemical attack [58].

GNPs dispersion analysis using X-ray Diffraction (XRD) Method

X-ray diffraction patterns of NR/EPDM blend nanocomposites are depicted in Fig. 8a, b for the effects of uGNPs and GNPs–PEI addition at lower (0.50 wt%) and higher (5.00 wt%) loadings. The presence of no peak for the unfilled NR/EPDM blend can be referred to as amorphous in nature in the macromolecule blend. For NR/EPDM blends filled with either uGNPs or GNPs–PEI, the dominant peak was observed ranging at $2\theta = 26^\circ\text{--}27^\circ$ corresponding to the basal spacing of graphite with an increase in relative peak intensity relative to the increase of GNPs filler addition (refer Fig. 8). The peak shifted to the left and reduced peak intensity were experienced by NR/EPDM blends filled with GNPs–PEI either at lower or higher loadings, indicating the possibility of improving GNPs dispersion due to non-covalent surface treatment. Polymeric adsorption successfully wrapped the surface of GNPs and created retention and isolation effects between the platelet bundles until the basal spacing characteristics of graphite crystallinity were reduced.

Table 4 Toluene uptake per 100 g rubber (Q) and rubber–filler interaction (Q_f/Q_g) ratio of NR/EPDM rubber blends filled with uGNPs and GNPs–PEI at various loadings

Output	System	0.00 wt%	0.25 wt%	0.50 wt%	1.00 wt%	3.00 wt%	5.00 wt%
Toluene uptake (Q)	A ^a	2.18	2.17	2.26	2.28	1.98	1.91
	B ^b	2.18	1.86	1.86	1.95	2.00	1.76
Q_f/Q_g	A	–	0.993	1.035	1.045	0.907	0.875
	B	–	0.849	0.849	0.890	0.917	0.806

^a NR/EPDM blends filled with uGNPs^b NR/EPDM blends filled with GNPs–PEI**Fig. 8** X-ray diffraction pattern of NR/EPDM blend nanocomposites at **a** lower GNPs loading (0.50 wt%); and **b** higher GNPs loading (5.00 wt%)

A less intense diffraction peak at 26° – 27° indicated the possibility of exfoliation, and probably had mixed with intercalated GNPs structures. PEI prevented steric reaggregation of platelets by adsorbing to the GNPs surface. This suggested that the disorder and loss of graphene layer regular structures or stacks are due to the adsorption of polymeric PEI layers onto the surface of GNPs through non-covalent interaction. Thus, the graphene tactoids were considered to be exfoliated, and the 0.3380-nm-thick d -spacing graphene platelets layers (Fig. 5) were dispersed at the molecular level into NR/EPDM blends matrices. The addition of non-

covalent-treated GNPs–PEI had introduced sort-off graphene platelets layer inclusion, which led to the loss of characteristically elevated chain orientation of the immiscible NR/EPDM blend system. Full-width-at-half-maximum (FWHM) values for uGNPs and GNPs–PEI were 0.5353 and 0.8028, respectively. GNPs–PEI experienced higher FWHM as compared to uGNPs. An increased FWHM value indicates successful layer separation between the GNPs platelets within NR/EPDM matrices, while the decreased d -spacing value of the NR/EPDM-filled GNPs–PEI blend compared to blends with uGNPs suggests the occurrence of polymeric adsorption on the GNPs surface by the PEI polymer.

Heat flow analysis using differential scanning calorimeter (DSC)

The effects of GNP surface modification on heat flow and glass transition temperature (T_g) were analyzed using endothermic scan traces of the first heating scan of filled and unfilled NR/EPDM blends. The samples were scanned within the temperature range from -65 to 150 °C, and the endotherms were overlaid and are depicted as in Fig. 9. The T_g is an indirect representation of the heterogeneous nature of polymeric blend [59]. The addition of surface modified and unmodified GNPs nanofiller at 5.00 wt% loading affected the thermal heat flow and shifted the T_g to some extent. The presence of GNPs in the form of uGNPs and GNPs–PEI had very much influenced the miscibility and compatibility of the hybrid blend system.

We found that uGNPs added at higher loading amounts had deteriorated the miscibility between the two rubber phases due to the presence of an intermediate T_g peak with a value located at between those of the NR and EPDM rubber. The peaks shifted from the original T_g peak of NR (-58.0 °C) and EPDM (-45.5 °C) rubber observed to slightly approach each other, indicating a partial miscibility phenomena between these rubber phases. Unmodified uGNPs nanofiller did not seem to be able to act as a compatibility enhancer for this rubber blend where it was presumed that the separation between the rubber phases had occurred which tended to diminish the overall performance of produced blends. This was further proved by the reduction of TS and EB for NR/EPDM blend filled with 5.00 wt% of uGNPs (refer Table 3).

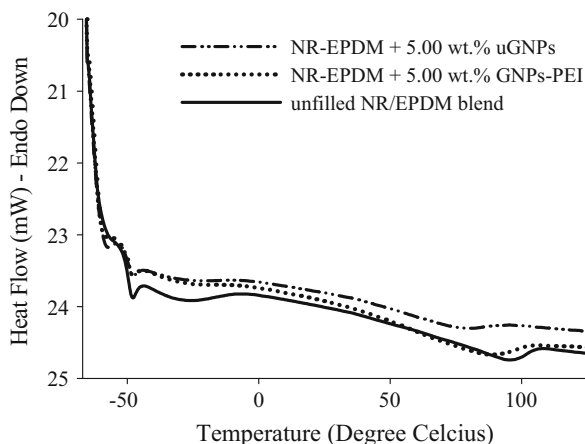


Fig. 9 Effects of GNPs surface modification to DSC endotherms for unfilled and filled NR/EPDM blends

Conversely, for the NR/EPDM blend filled with 5.00 wt% GNPs-PEI, the presence of nanofiller retained the occurrence of a single T_g peak with a slight temperature shift into -50.0 °C compared to the T_g of the miscible unfilled NR/EPDM blend at -49.0 °C. Modified GNPs-PEI surfaces introduced interactions between NR and EPDM rubber that might have occurred at the boundaries of their phases as a third phase, indicating improved miscibility and compatibility between them. Hence, the added GNPs-PEI successfully acted as inorganic compatibilizer which contributed further to the enhancement of resulting thermal and other properties of produced NR/EPDM blends filled with GNPs nanocomposites.

Thermal degradation and residue evaluation using thermogravimetric analysis (TGA)

The effects of GNPs surface modification to TGA and DTG thermal events for unfilled and filled NR/EPDM blend nanocomposites are depicted in Fig. 10a, b. Blends with a higher GNP loading of 5.00 wt% were selected to evaluate the contribution of GNPs surface treatment in affecting the thermal stability and degradation behavior of produced NR/EPDM blends. In descending order of thermal stability, it was found that the NR/EPDM blend with 5.00 wt% of uGNPs was more stable than the blend filled with 5.00 wt% of GNPs-PEI and the unfilled NR/EPDM blends with residue left based on the weight loss curves at 500 °C were about 12.8, 10.3, and 7.6 % for each respective blend (Fig. 10a).

The thermal event of the TGA and DTG curve pattern occurred in a similar manner for all blend systems with a distinct shift of decomposition percentage and DTG peaks, indicating the significant contribution of GNPs addition and the surface modification. Moreover, for all the blends tested, the triple degradation stage occurred at temperatures

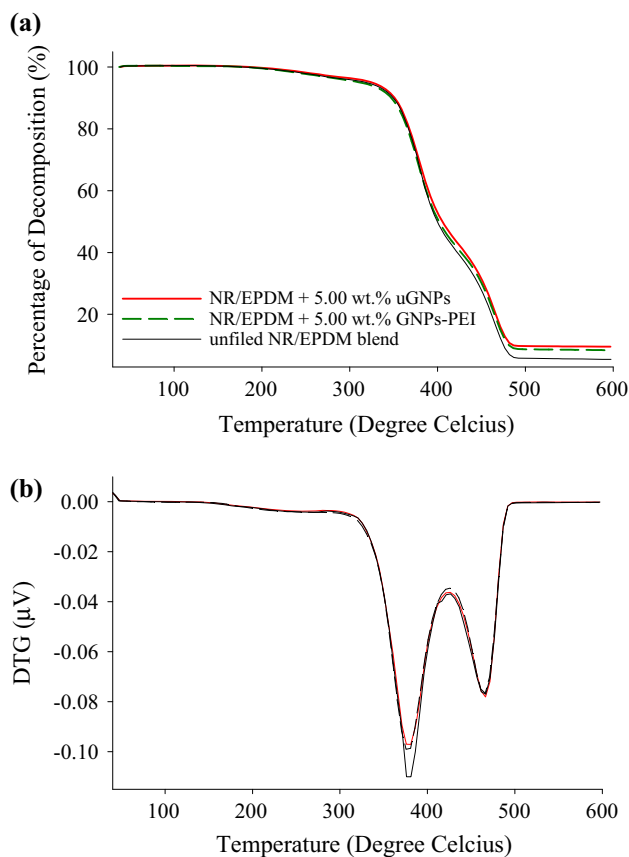


Fig. 10 Effects of GNPs surface modification to **a** TGA and **b** DTG thermal event for unfilled and filled NR/EPDM blends

ranging between 150–230, 240–440, and 440–500 °C as can be seen in the DTG curve (Fig. 10b). This phenomenon was attributed to a scission of the main chain of rubber phases with predominantly the evolution of carbon and oxygen groups resulting in the observed weight loss [60].

The absence of GNP nanofiller in unfilled NR/EPDM blends caused early degradation of the temperature set-point (T_d onset), as compared to filled NR/EPDM blends. GNPs themselves naturally have outstanding thermal properties and absolutely provide an added advantage to the blends filled with this nanofiller. However, it can be seen that the blends filled with modified GNPs-PEI experienced poorer thermal stability due to a lower degradation temperature onset and degradation temperature (low T_d onset and T_d) compared to blends with unmodified uGNP nanofiller. The presence of adsorbed polymeric layers on GNP surfaces, as observed through TEM micrographs (refer Fig. 5b), was responsible for providing a further degradation profile for GNPs-PEI. This involves the removal of water molecules due to increased hydrophilicity of the nanofiller, the decomposition of oxygen-containing groups due to excess OH and O from the adsorbed PEI, removal of ethylene and amino groups, and lastly the degradation of graphene. All these situations caused lesser

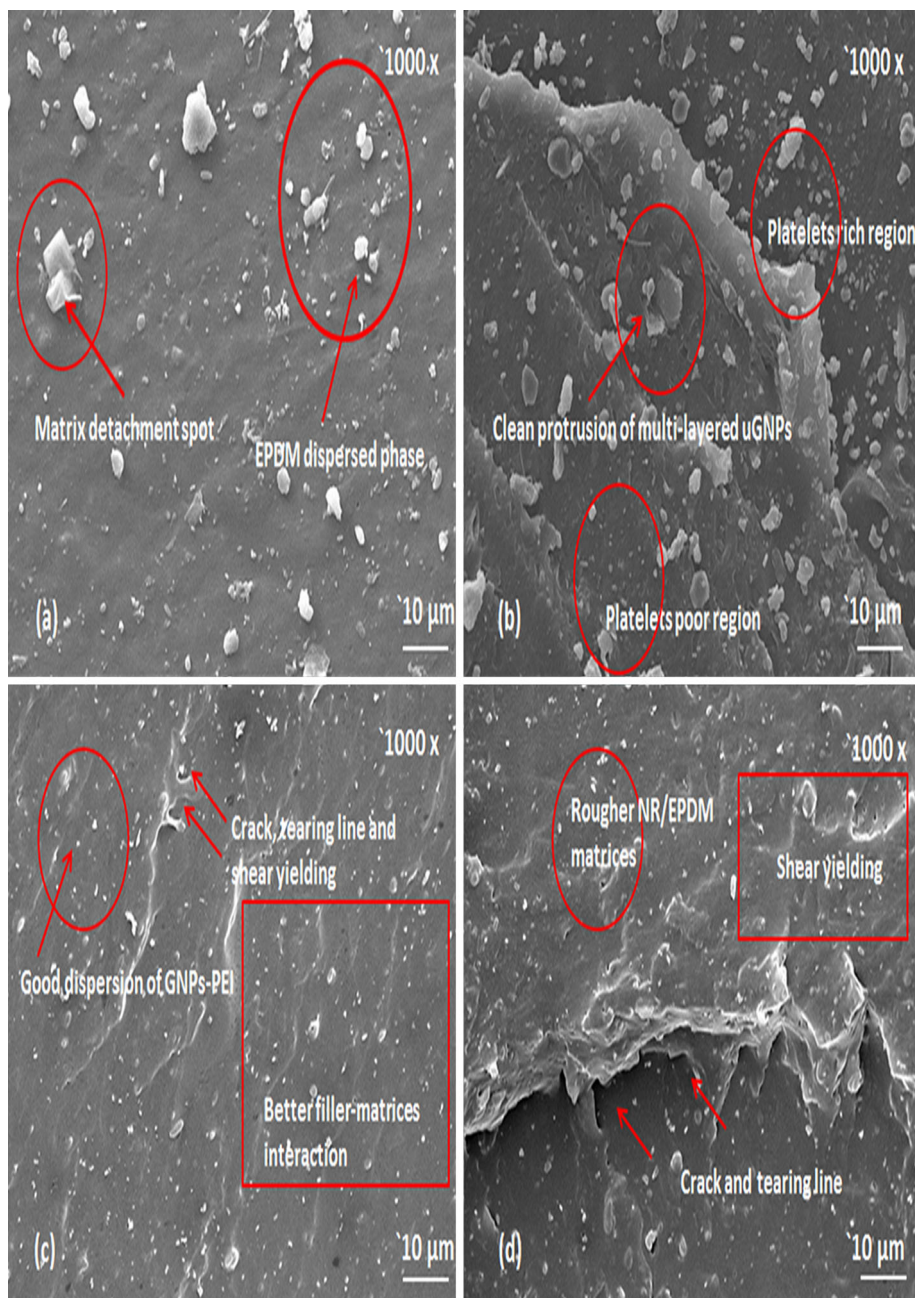
thermal stability for the blend with 5.00 wt% GNPs–PEI compared to blend filled with uGNPs at a similar loading.

In this case, unmodified uGNPs retained the excellent intrinsic thermal properties of graphene and increased the resistance of NR/EPDM blends to heat degradation. This can be explained by the presence of GNP layers protecting the underlying NR/EPDM rubber phases from degradation by acting as a physical barrier that limits the heat and mass transfer between the gas and carbonaceous condensed phase [60].

Tensile fracture morphology observation using scanning electron microscope (SEM)

The tensile-fractured morphologies, as observed by SEM observation, are depicted in Fig. 11a–d. There was a strong correlation between the resulting properties of the produced nanocomposite blends with the morphological characteristics and transformation of the fractured samples surface. The addition of GNP nanofiller significantly changed the fracture morphologies of the NR/EPDM rubber blend nanocomposites.

Fig. 11 Fractured surface morphology at 1 K of magnification for **a** unfilled NR/EPDM blend; **b** 5.00 wt% uGNPs–NR/EPDM blend; **c** 0.50 wt% GNPs–PEI–NR/EPDM blend; and **d** 5.00 wt% GNPs–PEI–NR/EPDM blend



The unfilled blend (Fig. 11a) revealed a homogeneous distribution of the EPDM dispersed phase embedded within the NR major phase. Fracture due to tensile loading caused several matrix detachments between NR and EPDM phases, providing a reason why the dispersed EPDM looked like it had not been fully wetted by a dominant NR phase. This unfilled blend also experienced smooth surface failure without the presence of any clear matrix yielding lines or shear ribs, indicating that no reinforcement mechanisms were involved for the unfilled NR/EPDM blend.

The fractured surface was rougher due to the presence of GNP nanofiller within the rubber matrix (Fig. 11b–d). Multilayer uGNPs nanofiller protruded cleanly from the fractured surface (Fig. 11b), indicating weak interfacial bonding, while the protruding GNPs–PEI nanofillers were thickly coated with adsorbed elastomeric blends, indicating strong interactions between the non-covalent-treated GNPs with rubber blends [61]. In addition, there was platelet clustering, which caused a decrease in the surface area in contact with the NR/EPDM blend, especially for the blend with a higher loading of untreated GNPs (>3.00 wt%) as depicted in Fig. 11b. The localized clustering of uGNPs nanofiller caused platelet-rich and platelet-poor regions in the nanocomposites that were responsible for lowering the tensile behavior performance of filled NR/EPDM blends.

However, for GNP–PEI-filled NR/EPDM nanocomposites at extremely low nanofiller content (0.50 wt%), we found that good dispersion of the nanosheet filler and strong interactions with the matrix polymer resulted in a substantial interphase zone around each sheet in which the mobility of the matrix polymer chains was altered [61]. Strong interfacial interactions between the blend matrices and GNPs–PEI caused crack lines and obvious matrix tearing lines due to pull-out between the rubber blend phases and the filler (Fig. 11c).

The nanoscale surface roughness resulted from the surface modification of GNPs–PEI enhanced mechanical interlocking with the polymer chains, consequently causing enhanced adhesion with the rubber blend. This contributed to an improvement in the mechanical tensile performance of NR/EPDM blends filled with GNPs–PEI nanocomposites (system B) as compared to NR/EPDM blend system filled with uGNPs (system A) at various filler loadings. Adsorption and absorption of polymeric poly(ethyleneimine) (PEI) onto GNP surfaces during non-covalent treatment introduced filler retention phenomena by altering the polymer mobility, caused by geometric constraints at the GNPs–PEI surface. This further promoted good interactions with NR/EPDM rubber blend matrices. In addition, considering the presence of hydroxyl groups across the surface of GNPs, hydrogen bonds may form between the nanofiller and the NR/EPDM rubber blends. The benefits of high surface area and nanoscale surface

roughness of GNPs–PEI enriched the surface chemistry of modified GNPs which may lead to stronger interfacial interactions with NR/EPDM rubber blend, thus substantially influencing the resultant properties of the elastomeric rubber blend.

Morphological transformations are clearly depicted in Fig. 11c, d for blends filled with GNPs–PEI at low (0.50 wt%) and high (5.00 wt%) loadings, respectively. It was quite difficult to image individually dispersed graphene sheets in fractured NR/EPDM rubber blend nanocomposites at low weight percentage of GNPs–PEI content. This may be due to polymeric adsorption by PEI which may isolate the GNPs through wrapping mechanisms that allow the interactions between an adsorb polymer from GNPs surfaces and the NR/EPDM blend matrices.

Overall, surface modification of GNPs uniformly dispersed the platelets within the rubber matrices with much better interface conditions, providing sufficient mechanical strength to resist external forces when fracturing the nanocomposites. Surface-treated GNPs may also act as an inorganic compatibilizer for improving the properties of immiscible NR/EPDM blends. The presence of poly(ethyleneimine) layers on GNP surfaces was able to perform a dual function in blend compatibilization and nanocomposite reinforcement. It may further promote interactions with the EPDM phase through hydrogen or van der Waals bonding, in addition forming strong linkages to rubber phases through polarity matching.

Conclusion

This study has shown that non-covalent treatment of GNPs with PEI can be successfully performed through a simplified polymeric adsorption method. Added GNPs–PEI was able to enhance the processability of NR/EPDM blends due to the presence of active surface chemistry and additional rubber–filler interactions induced by the presence of modified nanofiller to the blend matrices. GNPs–PEI also successfully acted as a reinforcement agent and an elasticity improver since adsorbed PEI onto GNPs introduced polar interactions between GNPs–PEI and NR/EPDM blends matrices. Further, enhanced platelet dispersion due to filler retention effects by the adsorbed PEI promoted the uniform force distribution during tensile loading. It was agreed that an enhancement in the resulted mechanical properties of filled NR/EPDM blends was not directly related to the crosslinking characteristic of NR/EPDM blends, but to other mechanisms introduced by the modified GNPs–PEI within the blend matrices. In addition, good dispersion of GNPs–PEI provided tortuosity path that enhanced blend resistance toward solvent penetration. GNPs–PEI introduced a polarity matching for strong

rubber–filler linkages that were responsible for nanoscale roughness in the fractured surfaces, which further supported a dual role of GNPs–PEI as an inorganic compatibilizer and reinforcement agent in enhancing the performance of NR/EPDM blends. In addition, modified GNPs–PEI was able to retain a single T_g , indicating a significant role of the surface treatment in affecting the miscibility of the blends. However, on the adverse side, the GNPs–PEI lessened the thermal stability of the blends due to early degradation onset of the PEI polymer. Hence, an enhancement strategy should be properly carried out to solve this issue.

Acknowledgements We greatly acknowledge the research funding from Fundamental Research Grant Scheme (FRGS) code FRGS/2012/FKP/TK04/02/1/F00132—Universiti Teknikal Malaysia Melaka (UTeM) for sponsoring this work. Our special gratitude to the Ministry of Education, Malaysia (MOE), Universiti Kebangsaan Malaysia (UKM), the Carbon Research Technology Research Group, Advanced Manufacturing Centre of Excellence Universiti Teknikal Malaysia Melaka, and the Malaysian Nuclear Agency (MNA) for the financial, technical, and supervisory support which made this work possible.

References

- Soldano C, Mahmood A, Dujardin E (2010) Production, properties and potential of graphene. *Carbon* 48:2127–2150
- Zhang YY, Wang CM, Cheng Y, Xiang Y (2011) Mechanical properties of bilayer graphene sheets coupled by sp^3 bonding. *Carbon* 49:4511–4517
- Li W, Tang X-Z, Zhang H-B, Jiang Z-G, Yu Z-Z, Du X-S, Mai Y-W (2011) Simultaneous surface functionalization and reduction of graphene oxide with octadecylamine for electrically conductive polystyrene composites. *Carbon* 49:4724–4730
- Wu H, Drzal LT (2012) Graphene nanoplatelet paper as a lightweight composite with excellent electrical and thermal conductivity and good gas barrier properties. *Carbon* 50:1135–1145
- Cao Y, Feng J, Wu P (2010) Preparation of organically dispersible graphene nanosheet powders through a lyophilization method and their poly(lactic acid) composites. *Carbon* 48:3834–3839
- Raza MA, Westwood AVK, Stirling C (2012) Effect of processing technique on the transport and mechanical properties of graphite nanoplatelet/rubbery epoxy composites for thermal interface applications. *Mater Chem Phys* 132:63–73
- Sridhar V, Lee I, Chun HH, Park H (2013) Graphene reinforced biodegradable poly(3-hydroxybutyrate-co-4-hydroxybutyrate) nano-composites. *eXPRESS Polym Lett* 7:320–328
- Fang M, Wang K, Lu H, Yang Y, Nutt S (2009) Covalent polymer functionalization of graphene nanosheets and mechanical properties of composites. *J Mater Chem* 19:7098–7105
- Stankovich S, Dikin DA, Piner RD, Kohlhaas KA, Kleinhammes A, Jia Y, Wu Y, Nguyen ST, Ruoff RS (2007) Synthesis of graphene-based nanosheets via chemical reduction of exfoliated graphite oxide. *Carbon* 45:1558–1565
- Kuilla T, Bhadra S, Yao D, Kim NH, Bose S, Lee JH (2010) Recent advances in graphene based polymer composites. *Prog Polym Sci* 35:1350–1375
- Ma J, Meng Q, Zaman I, Zhu S, Michelmore A, Kawashima N, Wang CH, Kuan HC (2014) Development of polymer composites using modified, high-structural integrity graphene platelets. *Compos Sci Technol* 91:82–90
- Mady MM, Mohammed WA, El-Guendy NM, Elsayed AA (2011) Interaction of DNA and polyethylenimine: Fourier-transform infrared (FTIR) and differential scanning calorimetry (DSC) studies. *Int J Phys Sci* 6:7328–7334
- Shan C, Wang L, Han D, Li F, Zhang Q, Zhang X, Niu L (2013) Polyethylenimine-functionalized graphene and its layer-by-layer assembly with Prussian blue. *Thin Solids Films* 534:572–576
- Wang F, Liu P, Nie T, Wei H, Cui Z (2013) Characterization of a polyamine microsphere and its adsorption for protein. *Int J Mol Sci* 14:17–29
- Wootthikanokkhan J, Tunjongnawin P (2003) Investigation of the effect of mixing schemes on cross-link distribution and tensile properties of natural–acrylic rubber blends. *Polym Test* 22:305–312
- Bitinis N, Verdejo R, Maya EM, Espuche E, Cassagnau P, Lopez-Manchado MA (2012) Physicochemical properties of organoclay filled polylactic acid/natural rubber blend bionanocomposites. *Compos Sci Technol* 72:305–313
- Kongsinlark A, Rempel GL, Prasassarakich P (2012) Synthesis of monodispersed polyisoprene–silica nanoparticles via differential microemulsion polymerization and mechanical properties of polyisoprene nanocomposite. *Chem Eng J* 193–194:215–226
- Sirisinha C, Saeoui P, Guaysomboon J (2004) Oil and thermal aging resistance in compatibilized and thermally stabilized chlorinated polyethylene/natural rubber blends. *Polym* 45:4909–4916
- Alipour A, Naderi G, Bakhshandeh GH, Vali H, Shokoohi S (2011) Elastomer nanocomposites based on NR/EPDM/organoclay: morphology and properties. *Int Polym Proc XXVI* 48–55:2011
- Arayaprane W, Rempel GL (2007) Properties of NR/EPDM blends with or without methyl methacrylate–butadiene–styrene (MBS) as a compatibilizer. *Int J Mater Struct Reliab* 5:1–12
- Botros SH, El Sayed AM (2001) Swelling behavior of NR/EPDM rubber blends under compression strain. *J Appl Polym Sci* 82:3052–3057
- Motaung TE, Luyt AS, Thomas S (2011) Morphology and properties of NR/EPDM rubber blends filled with small amounts of titania nanoparticles. *Polym Compos* 32:1289–1296
- Nabil H, Ismail H, Azura AR (2013) Compounding, mechanical and morphological properties of carbon-black-filled natural rubber/recycled ethylene propylene diene monomer (NR/R-EPDM) blends. *Polym Test* 32:385–393
- Sae-oui P, Sirisinha C, Thepsuwan U, Thapthong P (2007) Influence of accelerator type on properties of NR/EPDM blends. *Polym Test* 26:1062–1067
- Shehata AB, Afifi H, Darwish NA, Mounir A (2006) Evaluation of the effect of polymeric compounds as compatibilizers for NR/EPDM blend. *Polym Plast Technol Eng* 45:165–170
- Zaharescu T, Meltzer V, Vilcu R (1998) DSC studies on specific heat capacity of irradiated ethylene–propylene elastomers-II. EPDM. *Polym Degrad Stab* 61:383–387
- Arayaprane W, Rempel GL (2008) A comparative study of the cure characteristics, processability, mechanical properties, ageing, and morphology of rice husk ash, silica and carbon black filled 75:25 NR/EPDM blends. *J Appl Polym Sci* 109:932–941
- Zaharescu T, Meltzer V, Vilcu R (2000) Thermal properties of EPDM/NR blends. *Polym Degrad Stab* 70:341–345
- Sadayuki N, Tatsuo S (2007) Development of EPDM grades with good processability characteristics—specialized polymer design for anti-vibration rubber. *Sumitomo Kagaku* 2007-I:1–9
- Zhang H, Datta RN, Talma AG, Noordermeer JWM (2010) Maleic-anhydride grafted EPM as compatibilising agent in NR/BR/EPDM blends. *Eur Polym J* 46:754–766

31. El-Sabbagh SH (2003) Compatibility study of natural rubber and ethylene–propylene diene rubber blends. *Polym Test* 22:93–100
32. Ahmed K, Sirajuddin Nizami S, Raza NZ, Shirin K (2012) Cure characteristics, mechanical and swelling properties of marble sludge filled EPDM modified chloroprene rubber blends. *Adv Mater Phys Chem* 02:90–97
33. Halimatuddahlia Ismail H (2007) Thermoplastic elastomer based on PP/EPDM/ENR25 and PP/EPDM/NR blends. *Polym Plast Technol Eng* 43:357–368
34. Ismail H, Mathialagan M (2012) Comparative study on the effect of partial replacement of silica or calcium carbonate by bentonite on the properties of EPDM composites. *Polym Test* 31:199–208
35. Samaržija-Jovanović S, Jovanović V, Marković G, Konstantinović S, Marinović-Cincović M (2011) Nanocomposites based on silica-reinforced ethylene–propylene–diene–monomer/acrylonitrile–butadiene rubber blends. *Compos B* 42:1244–1250
36. Abd Razak J, Ahmad SH, Ratnam CT, Shueb MI, Mahamood MA, Yaakub J, Shamsuri SR, Mohamad N (2014) The effects of covalent treated graphene nanoplatelets surface modification to cure characteristic, mechanical, physical and morphological properties of NR/EPDM rubber blend nanocomposites. *Adv Environ Biol* 8:3289–3298
37. Abd Razak J, Ahmad SH, Ratnam CT, Mahamood MA, Lau KT, Ab Maulod HE, Munawar RF, Mohamad N (2015) Non-covalent polymeric wrapping of IGEPAL C0890 for graphene nanoplatelets (GNPs-C0890) filled NR/EPDM rubber blend nanocomposites. *Appl Mech Mater* 761:385–390
38. Abd Razak J, Ahmad SH, Ratnam CT, Mahamood MA, Yaakub J, Mohamad N (2015) Graphene nanoplatelets-filled NR/EPDM rubber blend: effects of GNPs loading on blend processability, mechanical properties and fracture morphology. *Polym Res J* 9:43–56
39. Ganguli S, Roy AK, Anderson DP (2008) Improved thermal conductivity for chemically functionalized exfoliated graphite/epoxy composites. *Carbon* 46:806–817
40. Abd Razak J, Ahmad SH, Ratnam CT, Mahamood MA, Yaakub J, Mohamad N (2015) Effects of EPDM-g-MAH compatibilizer and internal mixer processing parameters on the properties of NR/EPDM blends: an analysis using response surface methodology. *J Appl Polym Sci*. doi:10.1002/app.42199
41. Abd Razak J, Ahmad SH, Ratnam CT, Mahamood MA, Yaakub J, Mohamad N (2014) NR/EPDM elastomeric rubber blend miscibility evaluation by two-level fractional factorial design of experiment. *AIP Conf Proc* 1614:82–89
42. Ghoneim AM, Ismail MN (1999) Studies on EPDM/NR blends. I. Dielectric and mechanical properties. *Polym Plast Technol Eng* 38:979–995
43. Jovanović V, Samaržija-Jovanović S, Budinski-Simendić J, Marković G, Marinović-Cincović M (2013) Composites based on carbon black reinforced NBR/EPDM rubber blends. *Compos B* 45:333–340
44. Johnson PS (2001) Rubber processing: an introduction. Carl Hanser, Munich
45. Pasbakhsh P, Ismail H, Ahmad Fauzi MN, Abu Bakar A (2009) Influence of maleic anhydride grafted ethylene propylene diene monomer (MAH-g-EPDM) on the properties of EPDM nanocomposites reinforced by halloysite nanotubes. *Polym Test* 28:548–559
46. Ismail H, Shaari SM, Othman N (2011) The effect of chitosan loading on the curing characteristics, mechanical and morphological properties of chitosan-filled natural rubber (NR), epoxidised natural rubber (ENR) and styrene-butadiene rubber (SBR) compounds. *Polym Test* 30:784–790
47. Vijayalekshmi V (2009) Studies on natural rubber/clay nanocomposites: effect of maleic anhydride grafting of rubber. PhD Thesis, Cochin University of Science and Technology
48. Podstawka E, Ozaki Y, Proniewicz LM (2004) Part I: Surface-enhanced Raman spectroscopy investigation of amino acids and their homodipeptides adsorbed on colloidal silver. *Appl Spectrosc* 58:570–580
49. Stuart BH (2004) Infrared spectroscopy: fundamental and applications. Analytical techniques in the sciences. Wiley, London. doi:10.1002/0470011149
50. Geng Y, Liu MY, Li J, Shi XM, Kim JK (2008) Effects of surfactant treatment on mechanical and electrical properties of CNT/epoxy nanocomposites. *Compos A* 39:1876–1883
51. Sirqueira AS, Soares BG (2007) Compatibilization of natural rubber/EPDM blends by anhydride- and mercapto-functionalized copolymers. *J Macromol Sci Part B Phys* 46:639–650
52. Konar BB, Roy SK, Pariya TK (2010) Study on the effect of nano and active particles of alumina on natural rubber–alumina composites in the presence of epoxidized natural rubber as compatibilizer. *J Macromol Sci Part A Pure Appl Chem* 47:416–422
53. Tavakoli M, Katbab AA, Nazockdast H (2011) Effectiveness of maleic anhydride grafted EPDM rubber (EPDM-g-MAH) as compatibilizer in NR/organoclay nanocomposites prepared by melt compounding. *J Macromol Sci Part B Phys* 50:1270–1284
54. Basfar AA, Abdel-Aziz MM, Mofti S (2002) Influence of different curing systems on the physico-mechanical properties and stability of SBR and NR rubbers. *Radiat Phys Chem* 63:81–87
55. Zhang HB, Zheng WG, Yan Q, Jiang ZG, Yu ZZ (2012) The effect of surface chemistry of graphene on rheological and electrical properties of polymethylmethacrylate composites. *Carbon* 50:5117–5125
56. Guo J, Ren L, Wang R, Zhang C, Yang Y, Liu T (2011) Water dispersible graphene noncovalently functionalized with tryptophan and its poly(vinyl alcohol) nanocomposite. *Compos B* 42:2130–2135
57. George SC, Thomas S (2001) Transport phenomena through polymeric systems. *Prog Polym Sci* 26:985–1017
58. Kumnuantip C, Sombatsompop N (2003) Dynamic mechanical properties and swelling behaviour of NR/reclaimed rubber blends. *Mater Lett* 57:3167–3174
59. Mohamad N, Yaakub J, Abd Razak J, Yaakob MY, Shueb MI, Muchtar A (2014) Effects of epoxidized natural rubber (ENR-50) and processing parameters on the properties of NR/EPDM blends using response surface methodology. *J Appl Polym Sci* 40713:1–8
60. Cerezo FT, Preston CML, Shanks RA (2007) Morphology, thermal stability, and mechanical behavior of [poly(propylene)-grafted maleic anhydride]-layered expanded graphite oxide composites. *Macromol Mater Eng* 292:155–168
61. Ramanathan T, Abdala AA, Stankovich S, Dikin DA, Herrera-Alonso M, Piner RD, Adamson DH, Schniepp HC, Chen X, Ruoff RS, Nguyen ST, Aksay IA, Prud'Homme RK, Brinson RC (2008) Functionalized graphene sheets for polymer nanocomposites. *Nat Nanotechnol* 3:327–331